



1 **Heterogeneous reaction of HO₂ with airborne TiO₂ particles and its implication for**
2 **climate change mitigation strategies**

3

4 Daniel R. Moon¹, Giorgio S. Taverna², Clara Anduix-Canto¹, Trevor Ingham^{1,3}, Martyn P. Chipperfield^{2,3},
5 Paul W. Seakins^{1,3}, Maria-Teresa Baeza-Romero⁴, Dwayne E. Heard^{1,3*}

6

7 ¹ School of Chemistry, University of Leeds, Leeds, LS2 9JT, UK

8 ² School of Earth and Environment, University of Leeds, LS2 9JT, UK

9 ³ National Centre for Atmospheric Science, School of Chemistry, University of Leeds, Leeds, LS2 9JT, UK

10 ⁴ Escuela de Ingeniería Industrial, Universidad de Castilla-La Mancha, 45071, Toledo, Spain

11

12 * Corresponding author. Email: d.e.heard@leeds.ac.uk

13

14 **Abstract.**

15 One geoengineering mitigation strategy for global temperature rises resulting from the increased concentrations of
16 greenhouse gases is to inject particles into the stratosphere to scatter solar radiation back to space, with TiO₂ particles
17 emerging as a possible candidate. Uptake coefficients of HO₂, $\gamma(\text{HO}_2)$, onto sub-micrometre TiO₂ particles were
18 measured at room temperature and different relative humidities (RH) using an atmospheric pressure aerosol flow
19 tube coupled to a sensitive HO₂ detector. Values of $\gamma(\text{HO}_2)$ increased from 0.021 ± 0.001 to 0.036 ± 0.007 as the RH
20 was increased from 11% to 66%, and the increase in $\gamma(\text{HO}_2)$ correlated with the number of monolayers of water
21 surrounding the TiO₂ particles. The impact of the uptake of HO₂ onto TiO₂ particles on stratospheric concentrations
22 of HO₂ and O₃ was simulated using the TOMCAT three-dimensional chemical transport model. The model showed
23 that by injecting the amount of TiO₂ required to achieve the same cooling effect as the Mt. Pinatubo eruption,
24 heterogeneous reactions between HO₂ and TiO₂ would have a negligible effect on stratospheric concentrations of
25 HO₂ and O₃.

26

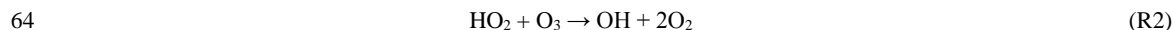
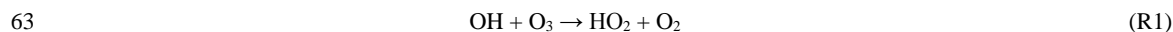


27 **1. Introduction**

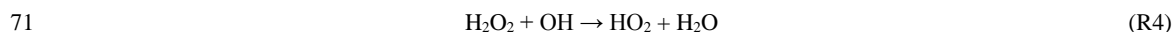
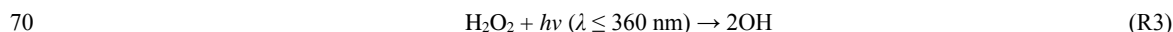
28 It has been suggested that injection of aerosols into the stratosphere in order to scatter solar radiation back to space
29 could be a possible solar radiation management scheme (Shepherd and Working Group on Geoengineering the
30 Climate, 2009). Such a scheme would have the effect of cooling the Earth's surface and serve as a measure to
31 mitigate enhanced global warming. A possible candidate for stratospheric injection is sulphuric acid aerosols as these
32 aerosols occur naturally in the stratosphere. These aerosols are formed by transport of precursors, e.g. SO₂ and
33 carbonyl sulphide (OCS), from the troposphere to the stratosphere (Holloway and Wayne, 2010), which form
34 sulphuric acid vapour that condenses onto particles. However, injection of these particles could have important
35 negative effects on the stratosphere through enhanced ozone depletion. Concentrations of sulphate aerosols can
36 increase dramatically as the result of volcanic eruptions. Following the eruption of Mt. Pinatubo in 1991, it was
37 estimated that around 30 Tg of H₂SO₄ was injected in the stratosphere, dramatically increasing stratospheric aerosol
38 loading and hence the available surface area for heterogeneous chemistry to occur. Following this volcanic event,
39 the average global lower tropospheric temperature decreased by 0.5 K (Dutton and Christy, 1992), however,
40 stratospheric ozone concentrations reached a record low in northern mid-latitudes (Dutton and Christy,
41 1992;McCormick et al., 1995) showing sulphate aerosols to be unsuitable for solar radiation management. Other
42 candidates for particle types, such as TiO₂, have been put forward due to their large refractive indices (Pope et al.,
43 2012), meaning that less stratospheric aerosol loading would be necessary to achieve the same level of cooling. The
44 refractive index of TiO₂ at 550 nm is 2.5 compared to a value of 1.5 for naturally occurring sulphate aerosols (Tang
45 et al., 2014). Assuming that the size of TiO₂ particles can be optimised, it has been reported that to achieve the same
46 cooling effect that sulphate aerosols had during the Mt. Pinatubo event, approximately three times less in mass, and
47 seven times less in volume of TiO₂ would be required compared with sulphuric acid (Pope et al., 2012). However,
48 the impacts of the presence of TiO₂ particles on stratospheric chemistry have to be determined before this kind of
49 geoengineering solution can be considered. Mineral dust particles are commonly found in the troposphere and
50 contribute the largest fraction to tropospheric aerosol loading in terms of mass (Textor et al., 2006;Huneus et al.,
51 2011). Typically TiO₂ (which is classified as a mineral) constitutes from 0.1% to 10% of overall atmospheric mineral
52 dust loading depending on the location of sources (Usher et al., 2003;Karagulian et al., 2006).

53 The heterogeneous chemistry of sulphate aerosols in the stratosphere is fairly well understood (Ammann et al., 2013);
54 for example the conversion of NO_x to nitric acid in the aerosol via N₂O₅ adsorption and reaction, and also the
55 activation of chlorine via the reaction of ClONO₂ with HCl to form Cl₂ and nitric acid within cold aerosols. However,
56 the heterogeneous reactivity of mineral particles, in particular TiO₂, is not as well understood. Removal and
57 production of trace gases in the stratosphere may significantly perturb concentrations of O₃, therefore it is important
58 when assessing the potential impact of such a solar radiation management scheme to evaluate the kinetics of likely
59 heterogeneous chemistry.

60 The hydroperoxyl radical, HO₂, is an important species within the stratosphere, being present at about 5 parts per
61 trillion per unit volume (pptv) around the tropopause, and is involved in a HO_x catalytic cycle responsible for about
62 40% of O₃ depletion in the lower stratosphere via the following reactions (Wennberg, 1994):



66 Moreover, HO₂ can also react with stratospheric ClO and BrO to produce HOCl and HOBr respectively, which can
67 be photolysed to produce further OH and atomic halogen species that can contribute to O₃ loss. HO₂ can undergo
68 self-reaction upon surfaces of mineral dust, which is thought to result in the generation of H₂O₂ (Matthews et al.,
69 2014), whose two predominant removal pathways are photolysis and reaction with OH (Versick et al., 2012):



72 Although the kinetics of the uptake of HO₂ onto Arizona Test Dust (ATD), a proxy of mineral dust, has been
73 previously investigated (Matthews et al., 2014;Bedjanian et al., 2013) the heterogeneous reaction of HO₂ with TiO₂
74 has not been studied. However, the kinetics of N₂O₅ uptake (Tang et al., 2014) and ClONO₂ (Tang et al., 2016) onto
75 TiO₂ have been studied. The heterogeneous reaction of N₂O₅ results in the conversion to reactive nitrogen oxides
76 (NO and NO₂) involved in a catalytic cycle that leads to significant O₃ depletion and non-reactive HNO₃. The reactive
77 uptake coefficient, γ , which is the probability that a species will collide with an aerosol and be removed by reaction,
78 was measured to be more than an order of magnitude larger for HO₂ onto ATD than for N₂O₅ and ClONO₂ onto TiO₂
79 sub-micron particles, and contrasting dependences of γ with relative humidities (RH) were observed. Therefore, by
80 analogy it is expected that HO₂ uptake onto TiO₂ may be faster than N₂O₅ uptake. ClONO₂ uptake by TiO₂ particles
81 resulted in similar values of γ , however, no dependency of γ with RH between 7 – 33% was observed.

82 In this investigation an aerosol flow tube coupled with a sensitive HO₂ detector based on chemical conversion
83 followed by laser-induced fluorescence detection of OH (George et al., 2013) has been used to study the kinetics of
84 the heterogeneous reaction of HO₂ with airborne TiO₂ nanoparticles at different RH. While it has been possible here
85 to study such kinetics over a range of RH representative to those typically found in the lower stratosphere (< 40%)
86 (Wennberg et al., 1994), experimental limitations meant that experiments were only conducted at room temperature
87 (~293 K). The TOMCAT off-line three-dimensional (3D) chemical transport model (Chipperfield; 1999) has also
88 been used to predict the likely impact of HO₂ uptake by TiO₂ particles on the stratospheric concentrations of HO₂
89 and O₃.

90

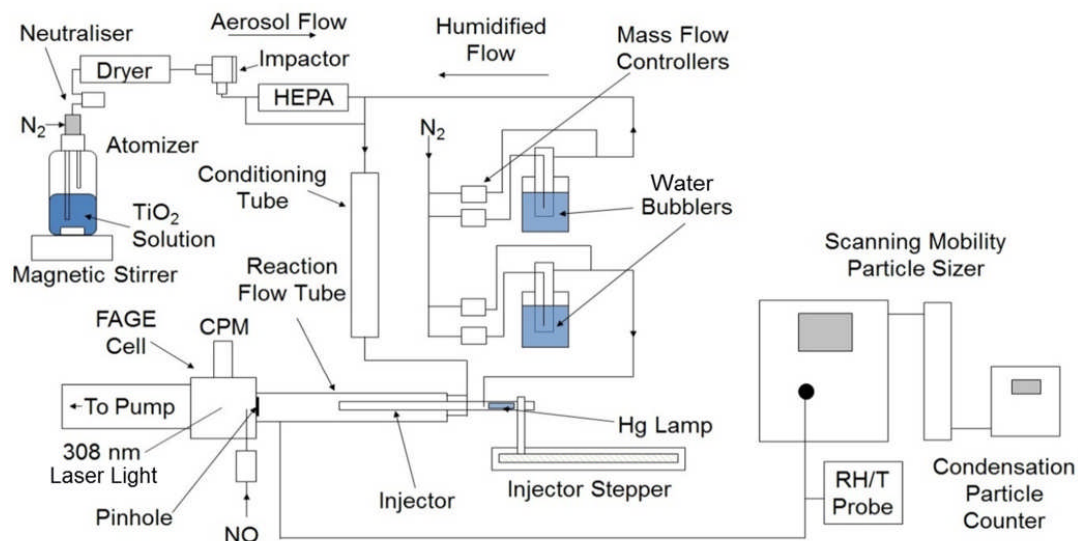
91 **2. Methods.**

92 **2.1. Overview of experimental apparatus**

93 The experimental setup deployed for this investigation is similar to other investigations of HO₂ uptake by aerosols
94 undertaken at the University of Leeds (George et al., 2013;Matthews et al., 2014;Lahey et al., 2016) therefore a



95 detailed description of the components of the experiment is not given. A schematic diagram of the experiment is
96 shown in Figure 1, and all experiments were undertaken at room temperature (~ 293 K) and under normal laboratory
97 levels of illumination. For some experiments the flow tube was covered with a black shield to eliminate light and no
98 differences in the results were observed.



99

100 **Figure 1.** Schematic diagram of the aerosol flow tube experiment. CPM: Channel Photomultiplier, HEPA: high-
101 efficiency particulate air filter, FAGE: fluorescence assay by gas expansion, RH/T: Relative Humidity/Temperature.

102

103 Compressed nitrogen, which had been passed through a gas purification system (TSI 3074B) consisting of particle
104 filters, a dryer and a carbon filter, was used as the carrier gas for the experiments. A humidified flow of TiO_2 particles
105 was introduced through two inlets located at the rear of the aerosol flow tube and the flow of HO_2 radicals enters the
106 flow tube via the movable injector. The total flow through the flow tube (107 cm length, 5.9 cm I.D.) was 5.4 L min^{-1}
107 which resulted in a Reynolds number of 130, and therefore is considered laminar as confirmed by radial
108 concentration gradient measurements of gases exiting the injector (George et al., 2013). Experiments consisted of
109 moving the injector using a linear drive (BSL Engineering 15 KR4610A) to different fixed positions along the flow
110 tube (30-70 cm from injector tip to HO_2 detector inlet in steps of 5 cm) corresponding to reaction times between ~ 8
111 and 20 s from the injector, with detection of HO_2 at the end of the flow tube. All gas flows within the experiment
112 were controlled using mass flow controllers (Brookes and MKS). The RH of the flow was measured using a probe
113 (Rotronics) in the exhaust of the flow tube, which itself was calibrated against a dew point hygrometer (Buck
114 Research Instruments CR-4).

115



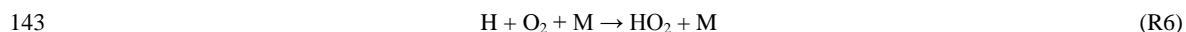
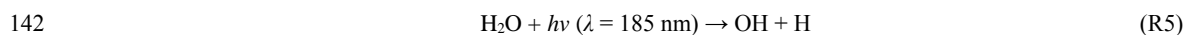
116 2.2. Aerosol Generation and Detection

117 A solution of TiO₂ (Aldrich Chemistry 718467, 99.5% Degussa, 5 g in 500 ml of Milli-Q water) was placed in a
118 commercial atomizer (TSI 3076) in order to produce a 1 L min⁻¹ flow entrained with TiO₂ particles, referred to as the
119 aerosol flow. The aerosol flow was then passed through a neutraliser (Grimm 5522) to reduce static wall losses, a
120 diffusion drier (TSI 3062) and an impactor (TSI 1035900) to ensure larger aerosols, beyond the detection range of
121 the SMPS (~ 750 nm diameter), do not enter the aerosol flow tube. A high-efficiency particulate air (HEPA, PALL
122 Life Sciences) filter situated within a by-pass loop was used to control the number concentration of particles entering
123 the aerosol flow tube. The aerosol flow was then mixed with a humidified flow of nitrogen (3 L min⁻¹) to control the
124 RH within the system. The RH of the humidified flow was altered by changing the ratio of dry nitrogen and nitrogen
125 passed through a water bubbler. This flow was then passed through a conditioning tube (residence time ~ 6 s) before
126 entering the aerosol flow tube to allow time for water adsorption onto the surface of the TiO₂ particles to equilibrate
127 at the given RH.

128 The total surface area of TiO₂ particles available for heterogeneous reaction with HO₂ was measured with a SMPS
129 instrument from the flow exiting the aerosol flow tube. Previous experiments showed that there is a negligible loss
130 of aerosols during the transit of the flow tube (George et al., 2013). The SMPS consisted of a Differential Mobility
131 Analyzer (DMA, TSI 3080, 3081) that creates a monodisperse flow of aerosols based on their electrical mobility
132 which is related to their size. A condensation particle counter (CPC, TSI 3775) connected in parallel to the DMA
133 quantified particle number concentrations. These two instruments connected in parallel can be used to create an
134 aerosol size distribution from which the total surface area and average radius of particles can be calculated by making
135 the assumption that particles are spherical (as demonstrated experimentally in section 3.2 below). The average
136 diameter of the particles is 136 nm and 173 nm at RH = 11% and 37%, respectively.

137 2.3 HO₂ Generation and Detection

138 HO₂ radicals were produced within the movable injector (110 cm length, 1.9 cm O.D., 1.6 cm I.D.) by passing a 1.3
139 L min⁻¹ humidified flow of nitrogen (consisting of a mixture of 0.9 L min⁻¹ of dry N₂ and 0.4 L min⁻¹ N₂ passed
140 through a water bubbler) containing trace amounts of oxygen over a mercury lamp (L.O.T.-Oriel 6035) via the
141 following reactions:



144 OH is also created by the photolysis of water vapour in R5, but no OH was observed exiting the injector, presumably
145 owing to rapid losses at the walls of the injector. HO₂ was sampled by a 0.7 mm diameter pinhole at the end of the
146 flow tube, and after chemical conversion to OH by addition of excess NO (50 sccm, BOC, 99.5 %) just inside the
147 pinhole, laser induced fluorescence (LIF) at low-pressure (the fluorescence assay by gas expansion (FAGE) technique
148 (Heard and Pilling, 2003)) was used to measure OH. The relative LIF signal from converted HO₂ was calibrated
149 using an established method (Winiberg et al., 2015) developed for field measurements of OH and HO₂ radicals.
150 Hence the experiment is able to measure the absolute concentration of HO₂ during passage from the injector to the



151 sampling inlet. The $Q_1(2)$ line of the OH ($A^2\Sigma^+ v'=0 - X^2\Pi_1- v''=0$) transition at ~ 308 nm was used to detect OH.
152 A Nd:YAG pumped dye laser (JDSU Q201-HD Q-series, Sirah Cobra Stretch) was used to produce the required 308
153 nm radiation (line width ~ 0.1 cm $^{-1}$) at a pulse repetition rate of 5 kHz. As the flows through the movable injector
154 (1.3 L min $^{-1}$) and mercury lamp current (20 mA) were kept constant, it is assumed that the initial HO $_2$ concentration,
155 [HO $_2$] $_0$ (defined in this investigation as [HO $_2$] at the first injector position, i.e. 30 cm downstream of the injector),
156 determined by calibration to be 1.6×10^9 molecule cm $^{-3}$, was the same for all experiments. These HO $_2$ concentrations
157 are ~ 50 times higher than typical levels in the sunlit stratosphere (Wennberg et al., 1994). A reference fluorescence
158 cell, in which a large concentration of OH was generated and detected by LIF, was used to facilitate the identification
159 of OH lines and tune the laser wavelength. The FAGE cell was continuously evacuated using a combination of a
160 rotary pump (Edwards, model E1M80) and a roots blower (EH1200), and was kept at 0.8–0.9 Torr, which was
161 monitored using a capacitance monitor (Tylan General, CDC 11).

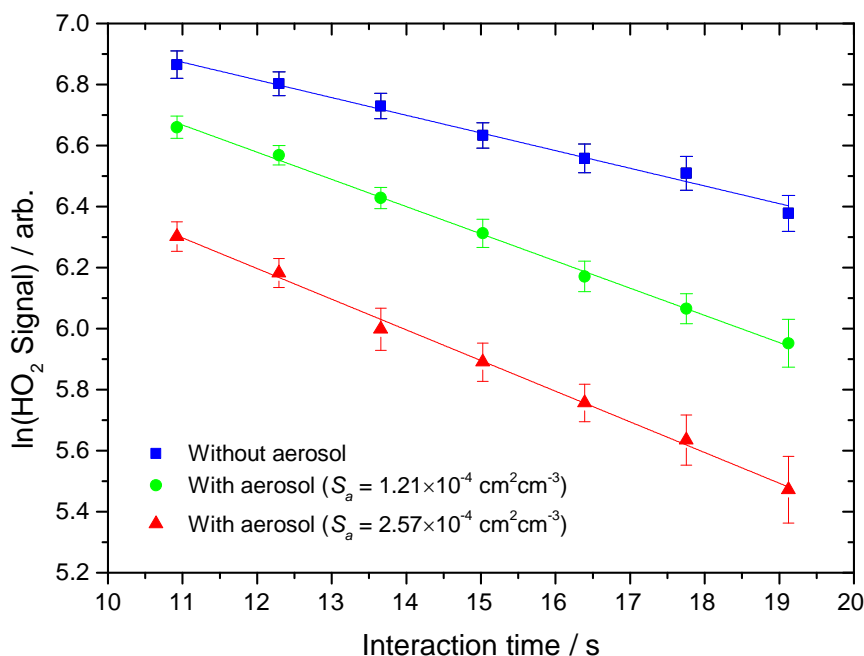
162 **2.4. Experimental Procedure and Data Analysis**

163 The HO $_2$ signal was measured at 8 positions as the moveable injector was drawn back from 30 to 70 cm using the
164 linear stepper drive and again as the moveable injector was pushed forwards back to its initial position. The HO $_2$
165 signal was averaged over 20 s (average of twenty 1 s measurement points, each corresponding to 5000 laser shots) at
166 each injector position with a 22 s delay between measurements at each injector position in order to allow time for
167 mechanical vibrations to subside, and to ensure a full flush of the aerosol flow tube so that the LIF signal corresponds
168 to HO $_2$ emitted from the injector position being measured. The laser power was recorded for each injector position
169 and used to normalise the HO $_2$ signal to correct for any fluctuations in laser power ($< 5\%$). The HO $_2$ signals with the
170 injector moving forwards and backwards were then averaged, and this procedure repeated six times with varying
171 concentrations of aerosols present in the aerosol flow tube. The wall loss rate of HO $_2$ (k_{wall}) was determined by
172 recording the HO $_2$ decay in the absence of aerosols, but at the same RH, and was repeated four times for each
173 experiment.

174 The HO $_2$ concentration as a function of time along the flow tube can be expressed as:

$$175 \quad \ln[\text{HO}_2]_t = \ln[\text{HO}_2]_0 - k_{\text{obs}} t \quad (\text{Eqn. 1})$$

176 where [HO $_2$] $_t$ and [HO $_2$] $_0$ are concentrations of HO $_2$ at time t and $t = 0$ respectively, and k_{obs} is the observed pseudo-
177 first-order rate coefficient for HO $_2$ uptake. As the HO $_2$ signal is directly proportional to the concentration of HO $_2$,
178 the gradient of a plot of $\ln(\text{HO}_2 \text{ Signal})$ against time (calculated from the injector position and measured flow rate)
179 yields k_{obs} , as shown in Figure 2.



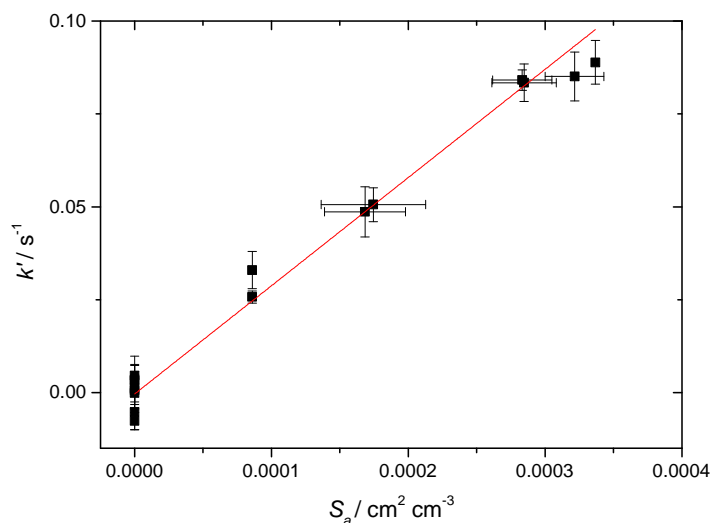
180

181 **Figure 2.** Measured HO₂ signal at different interaction times, in the presence of TiO₂ particles (surface area density
 182 $1.21 \times 10^{-4} \text{ cm}^2 \text{ cm}^{-3}$ and $2.57 \times 10^{-4} \text{ cm}^2 \text{ cm}^{-3}$, green circles and red triangles respectively) and in their absence (blue
 183 squares). The RH in the aerosol flow tube was 11%, the lowest used in this study. The lines represent linear-least
 184 squares fits to the data yielding $k_{\text{obs}} = 0.079 \pm 0.005 \text{ s}^{-1}$ and $k_{\text{obs}} = 0.093 \pm 0.003 \text{ s}^{-1}$ (aerosols present, green circles
 185 and red triangles respectively) and $0.049 \pm 0.003 \text{ s}^{-1}$ (no aerosols, k_{wall}).

186 The flow tube was coated with halocarbon wax (Halocarbon Products Corporation, Halocarbon Wax Series 600) to
 187 reduce HO₂ wall loss rate (k_{wall}) and an average of k_{wall} from several determinations in the absence of aerosols was
 188 subtracted from k_{obs} . A correction (typically about 30%) to account for non-plug flow conditions in the aerosol flow
 189 tube using the procedure outlined by Brown (Brown, 1978) was applied to yield, k' , the pseudo-first-order loss of
 190 HO₂ by heterogeneous reaction with TiO₂ particles. The relationship between k' and total surface area of TiO₂
 191 particles (S_a) can be expressed as (George et al., 2013):

$$192 \quad k' = \frac{w_{\text{HO}_2} \gamma_{\text{obs}} S_a}{4} \quad (\text{Eqn. 2})$$

193 where w_{HO_2} is the mean velocity of HO₂ ($\sim 435 \text{ ms}^{-1}$ at 293 K) and γ_{obs} is the observed reactive uptake coefficient,
 194 obtained from a plot of k' versus S_a , an example of which is given in Figure 3. γ_{obs} was in turn corrected (typically
 195 $\sim 1\%$) to account for the gas diffusion limitation (Fuchs and Sutugin, 1970), to yield $\gamma(\text{HO}_2)$.



196

197 **Figure 3.** First order rate coefficient for loss of HO₂ due to heterogeneous reaction with TiO₂ particles at different
198 total surface areas for T = 296 K and RH = 37%. The gradient yielded a value of $\gamma(\text{HO}_2) = (2.68 \pm 0.01) \times 10^{-2}$, with
199 the uncertainty representing 2 σ random errors from the fit (95% confidence limits).

200 2.5. TOMCAT Model Description

201 The TOMCAT off-line three-dimensional (3D) chemical transport model (CTM) (Chipperfield, 1999, 2006) has been
202 used to predict the impact of the heterogeneous reaction of TiO₂ with HO₂ to stratospheric concentrations of O₃ and
203 HO₂. The model has been widely used in previous studies of stratospheric chemistry and performs well in reproducing
204 stratospheric ozone and the trace species which control its distribution (Chipperfield et al., 2015). The model includes
205 a detailed treatment of stratospheric chemistry of O_x, HO_x, NO_y, Cl_y and Br_y species along with the main source
206 gases. The model has a comprehensive gas-phase chemistry scheme and includes a number of heterogeneous
207 reactions on stratospheric sulphate aerosols and polar stratospheric clouds (Chipperfield, 1999).

208 The loss rate of HO₂ due to heterogeneous reaction with TiO₂ was included in the model as:

$$209 \quad k = 0.25 S_a w_{\text{HO}_2} \gamma(\text{HO}_2) \quad (\text{Eqn. 3})$$

210 where S_a is the surface area density of TiO₂, and w_{HO_2} and $\gamma(\text{HO}_2)$ are defined above. Three TOMCAT simulations
211 were performed at a horizontal resolution of $5.6^\circ \times 5.6^\circ$ and 32 levels from the surface to ~ 60 km. The model was
212 forced with wind and temperature fields from the European Centre for Medium-Range Weather Forecasts (ECMWF)
213 ERA-Interim reanalyses and integrated for 2 years from January 2007 until December 2008, initialised with the
214 output from a standard TOMCAT run which had spun-up from 1977. More information on the model experiments is
215 given in Section 3.3.

216

217



218 3. Results and Discussion

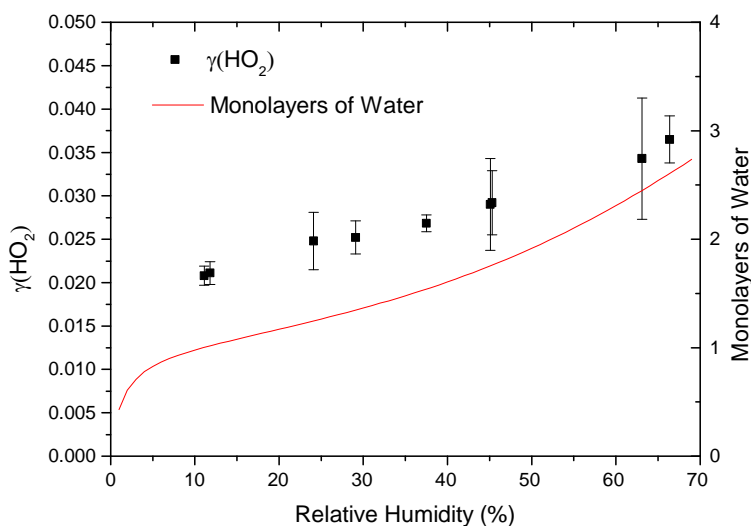
219 3.1. The reactive uptake coefficient dependence with relative humidity

220 The reactive uptake coefficient for HO₂ radicals, $\gamma(\text{HO}_2)$, onto TiO₂ particles was determined at eight different RH
221 (11 - 66%), as shown in Figure 4 and summarised in Table 1. The number of monolayers of water adsorbed onto the
222 surface of TiO₂ particles has been previously determined experimentally by transmission FTIR spectroscopy
223 (Goodman et al., 2001), and is also shown as a function of RH in Figure 4.

224 **Table 1.** Reactive HO₂ uptake coefficients, $\gamma(\text{HO}_2)$, for TiO₂ particles at different RH.

RH (%) \pm 1.0	$\gamma(\text{HO}_2) \times 10^{-2}$
11.1	2.08 ± 0.11
11.8	2.11 ± 0.13
24.9	2.48 ± 0.33
29.1	2.54 ± 0.18
37.5	2.68 ± 0.09
45.1	2.90 ± 0.53
45.3	2.92 ± 0.37
63.1	3.43 ± 0.27
66.4	3.65 ± 0.70

225



226

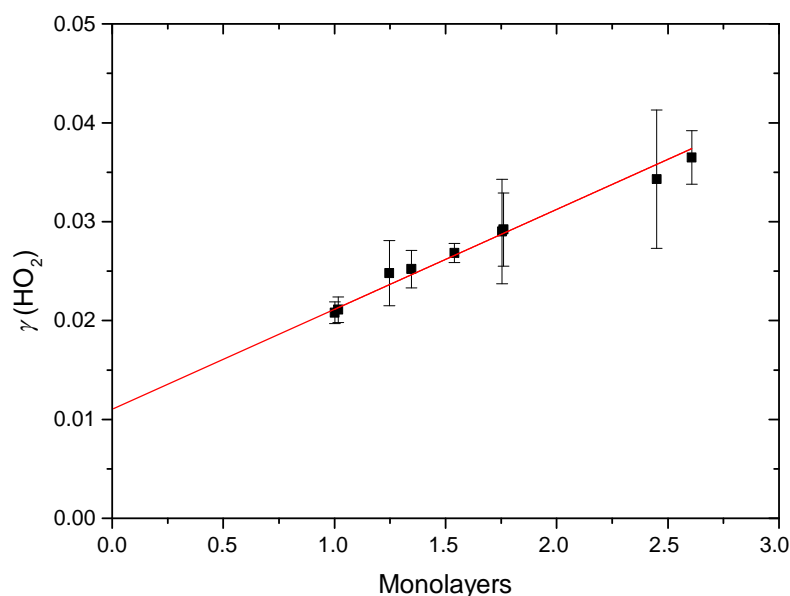
227 **Figure 4.** Reactive uptake coefficients of HO₂, $\gamma(\text{HO}_2)$, onto airborne TiO₂ particles (black squares, left y axis) at
228 different RH for $T = 295 \pm 2$ K. The number of monolayers of the adsorbed water on TiO₂ particles (red curve, right
229 y axis) at 296 K is also plotted as a function of RH, determined using FTIR spectroscopy (Goodman et al., 2001).



230 The results clearly show a positive dependence of $\gamma(\text{HO}_2)$ across the range of RH investigated, and as shown in Figure
231 5, $\gamma(\text{HO}_2)$ correlates well with the number of monolayers of water adsorbed onto the TiO_2 particles, V/V_m , determined
232 by Goodman *et al.* (2001), and which was parameterised by Eqn. 4:

$$233 \quad \frac{V}{V_m} = \left[\frac{c \left(\frac{P}{P_0} \right)}{1 - \left(\frac{P}{P_0} \right)} \right] \left[\frac{1 - (n+1) \left(\frac{P}{P_0} \right)^n + n \left(\frac{P}{P_0} \right)^{n+1}}{1 + (c-1) \left(\frac{P}{P_0} \right) - c \left(\frac{P}{P_0} \right)^{n+1}} \right] \quad (\text{Eqn. 4})$$

234 where V is the volume of gas (water vapour) adsorbed at equilibrium pressure P , V_m is volume of gas necessary to
235 cover the surface of the adsorbent TiO_2 particles with a complete monolayer, P is the equilibrium pressure of the
236 adsorbing gas, P_0 is the saturation vapour pressure of the adsorbing gas at that temperature, c is a temperature-
237 dependent constant related to the enthalpies of adsorption of the first and higher layers and n is the asymptotic limit
238 of monolayers (~ 8).



239

240 **Figure 5.** Variation of the reactive uptake coefficient, $\gamma(\text{HO}_2)$, with the number of monolayers of water surrounding
241 TiO_2 particles (as determined by Goodman *et al.*, 2001) for $T = 295 \pm 2$ K. The red line represents a linear least-
242 squares fit to the data ($r^2 = 0.987$).

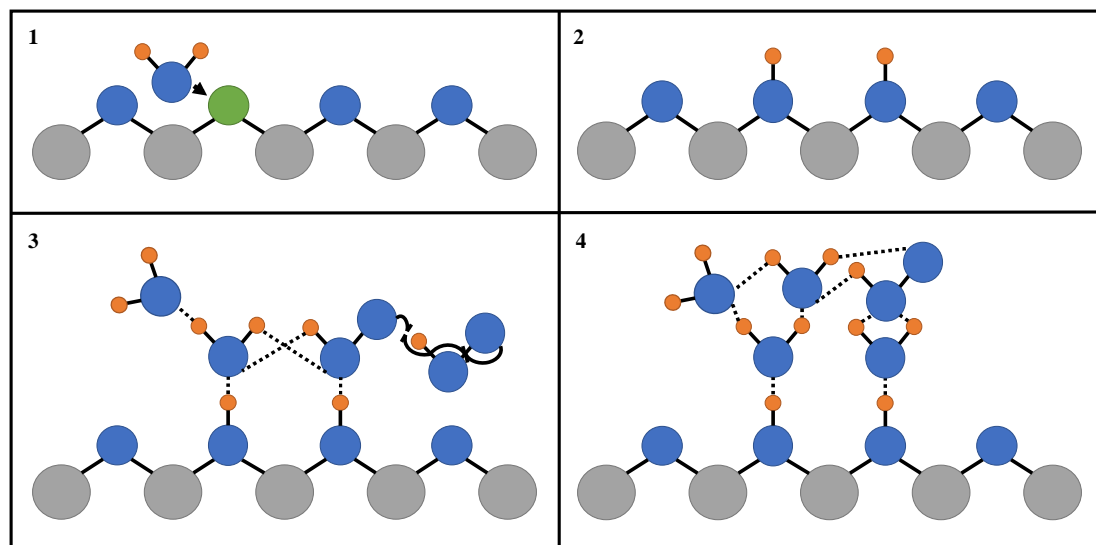
243

244 Wall losses of HO_2 also increase as RH is increased within the aerosol flow tube, and so in the absence of aerosols,
245 the $[\text{HO}_2]$ for a given distance from the injector will decrease with RH. Previous work in this laboratory has shown
246 that $\gamma(\text{HO}_2)$ for uptake on ATD aerosols increases as the $[\text{HO}_2]$ is lowered (Matthews *et al.*, 2014), and hence some
247 of the positive dependence of $\gamma(\text{HO}_2)$ with RH shown in Figure 4 might be expected simply owing to the $[\text{HO}_2]$
248 impinging on the aerosol for a given injector position decreasing with RH. To investigate this further, uptake onto



249 TiO_2 at RH = 11% was measured as a function of $[\text{HO}_2]_0$ exiting the injector, and $\gamma(\text{HO}_2)$ increased from 2.08×10^{-2}
250 to 2.72×10^{-2} as $[\text{HO}_2]_0$ was decreased from 1.6×10^9 molecule cm^{-3} to 8.9×10^8 molecule cm^{-3} . However, the wall
251 loss rate for HO_2 only increased from 0.049 to 0.079 s^{-1} across the entire range of RH (11% to 66%) resulting in only
252 a small change in $[\text{HO}_2]$, decreases of $\sim 2.6 \times 10^8$ molecule cm^{-3} and $\sim 2.7 \times 10^8$ molecule cm^{-3} at the first and last
253 injector position, respectively. In previous studies of HO_2 uptake onto ATD (Matthews et al., 2014) it was shown
254 that the increase of $\gamma(\text{HO}_2)$ with decreasing $[\text{HO}_2]$ is linear. Therefore, assuming the same behaviour for uptake onto
255 TiO_2 particles, the expected change in $\gamma(\text{HO}_2)$ as a result of RH increasing from 11-66% due only to a change in
256 initial HO_2 concentration is only $\Delta\gamma(\text{HO}_2)=0.0023$ (or $\sim 6\%$ of the averaged measured $\gamma(\text{HO}_2)$ across this range).
257 Hence the 175 % increase in $\gamma(\text{HO}_2)$ observed in Figure 4 across this range of RH is due to another reason.

258 Figure 5 shows that, for the range of RH studied, $\gamma(\text{HO}_2)$ is a linear function of the number of monolayers of water
259 surrounding a TiO_2 particle, suggesting that water plays a role in the reactive HO_2 uptake process on TiO_2 particles.
260 Studies using ambient pressure photoelectron spectroscopy (APPEs) (Yamamoto et al., 2008; Ketteler et al., 2007)
261 have shown that water adsorption on rutile, a polymorph of TiO_2 (110), occurs in distinct steps, as illustrated in Figure
262 6.

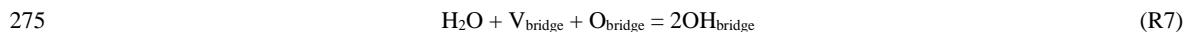


263

264 **Figure 6.** Simplified diagram of the important steps of HO_2 reactive uptake onto the surface of TiO_2 . Grey circles
265 = Ti, blue circles = O, orange circles = H, green circles = V_{bridge} , solid black lines = chemical bond and dashed lines
266 = hydrogen bond. Panel 1 shows the diffusion of water molecule towards a bridging O vacancy. Panel 2 shows the
267 resultant formation of two neighbouring bridging OH groups at the original site of the O vacancy. Panel 3 shows
268 the bridging OH groups acting as anchoring sites for water and HO_2 adsorption via hydrogen bonding leading to
269 multilayer water adsorption and HO_2 self-reaction via an Eley-Rideal type mechanism. Panel 4 shows the build up
270 of a more extensive hydrogen bonded network as more water molecules adsorb onto the particle, which stabilises
271 HO_2 increasing its desorption lifetime and hence probability that it will react.



272 First, water molecules dissociate at O-vacancies (V_{bridge}) in bridge sites, producing a stoichiometric amount of
 273 adjacent bridging OH groups ($\text{OH}_{\text{bridge}}$) equal to twice the initial vacancy concentration upon initial exposure of rutile
 274 to water vapour:



276 This step takes place even at very low RH, with these bridging OH groups acting as nucleation sites for subsequent
 277 water adsorption by anchoring water molecules to form strongly bound $\text{OH-H}_2\text{O}$ complexes. The $\text{OH-H}_2\text{O}$
 278 complexes continue to act as nucleation centres for further water adsorption. The wetting properties of TiO_2 (110)
 279 are thus driven by moderate amounts of strongly attractive OH sites that nucleate water molecules. These $\text{OH-H}_2\text{O}$
 280 complexes have a relatively high enthalpy of adsorption for water of -72 kJ mol^{-1} (Ketteler et al., 2007), whereas
 281 additional adsorption of water beyond a monolayer of water coverage is more characterised by enthalpies associated
 282 with the bulk enthalpy of water condensation (-45 kJ mol^{-1}) (Chen et al., 2012), explaining the variation of the number
 283 of monolayers of water with RH shown in Figure 4. Computational studies (Aloisio and Francisco, 1998) showed
 284 that in the gas-phase HO_2 can also readily form complexes with water through hydrogen bonding with a binding
 285 energy of 28.9 kJ mol^{-1} . The observed correlation of $\gamma(\text{HO}_2)$ with the number of monolayers of water surrounding
 286 TiO_2 particles could be explained by two effects. An increase in the network of hydrogen bonding would increase
 287 the stability of a molecular system, $\sim 20.9 \text{ kJ mol}^{-1}$ for each hydrogen bond (Joshi and Ghanty, 2013), or that simply
 288 more HO_2 can adsorb onto the particle surface as the number of available sites for hydrogen bonding increases. An
 289 increase in the adsorption lifetime of HO_2 owing to the more extended H-bonding network (Joshi and Ghanty, 2013)
 290 will result in an increased probability of HO_2 reacting with another HO_2 , increasing the value of $\gamma(\text{HO}_2)$:



292 For up to ~ 2 monolayers of H_2O , an Eley-Rideal (ER) mechanism of a gas phase HO_2 molecule reacting an adsorbed
 293 HO_2 is more likely than for two adsorbed HO_2 molecules diffusing together to react via a Langmuir-Hinshelwood
 294 (LH) mechanism. The coverage of V_{bridge} across the surface of TiO_2 (110) is 0.125 monolayers (i.e. one vacancy for
 295 every eight unit cells) (Ketteler et al., 2007) meaning water will initially adsorb onto the surface of the particle in
 296 clusters. As the binding energy of the HO_2 water complex is fairly high, the rate of HO_2 diffusion across the surface
 297 after the initial adsorption at a bridging site will be slow, making a LH type mechanism seem unlikely. Above ~ 2
 298 monolayers, the adsorbed water clusters will begin to interact with each other via an extended H-bonded network
 299 more characteristic of bulk liquid water, allowing HO_2 to diffuse around the thin surface film of water with
 300 thermodynamic properties similar to liquid water (Ketteler et al., 2007).

301 The superoxide ion, O_2^- , which is the conjugate base of HO_2 , reacts with HO_2 over a hundred times quicker than with
 302 HO_2 via:



304 It is unlikely that O_2^- will form readily on the surface of the particle at low coverages of water. O_2^- can form on
 305 surfaces via direct surface-oxygen electron transfer, photo-induced electron transfer, surface intermolecular electron



306 transfer or decomposition of hydrogen peroxide (H_2O_2) (Anpo et al., 1999). The dissociation of HO_2 to O_2^- occurs in
307 bulk liquid ($pK_a = 4.7$, (Thornton and Abbatt, 2005)), however, water surrounding the particles only begins to acquire
308 liquid like properties once the coverage of water is greater than ~ 2 monolayers. If significant formation of O_2^- does
309 occur above ~ 2 monolayers of H_2O , then owing to its much higher reactivity, some deviation from linearity of $\gamma(\text{HO}_2)$
310 versus monolayers of water (Figure 5) might be expected. However, this was not observed, although the number of
311 data points is very limited.

312

313 3.2. Comparison of $\gamma(\text{HO}_2)$ with literature values

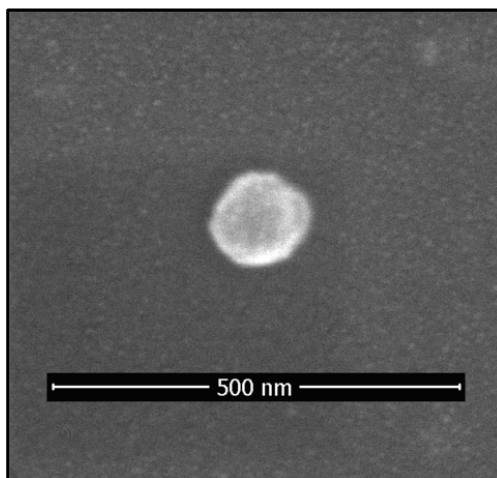
314 There are previous studies of HO_2 uptake onto ATD (Matthews et al., 2014), a proxy for mineral dust, and both N_2O_5
315 (Tang et al., 2014) and ClONO_2 (Tang et al., 2016) uptake onto TiO_2 particles. Values of $\gamma(\text{HO}_2)$ measured for ATD
316 are comparable to those measured onto TiO_2 particles at similar concentrations of HO_2 in the aerosol flow tube
317 ($\gamma(\text{HO}_2)_{\text{ATD}} \sim 0.008 - 0.030$). For ATD, $\gamma(\text{HO}_2)$ was only determined at 4 values of RH, but a general increase with
318 RH was observed (although there was a dip around $\text{RH} = 50\%$ before a further increase), consistent with HO_2 uptake
319 being driven by the number of defects in the crystal lattice of mineral dust surfaces which provides bridging OH
320 groups upon exposure to water and subsequently by the number of monolayers of water adsorbed onto the surface of
321 such aerosols. The number of monolayers of water on the ATD surface at different RH has been determined
322 (Gustafsson et al., 2005), and also showed a general increase with RH but with a shoulder around $\text{RH} = 50\%$ where
323 the observed $\gamma(\text{HO}_2)$ also contained a small dip.

324 Values of $\gamma(\text{N}_2\text{O}_5)$ (Tang et al., 2014a; and corrigendum Tang et al. 2014b) and $\gamma(\text{ClONO}_2)$ (Tang et al., 2016) onto
325 TiO_2 particles were an order of magnitude lower than $\gamma(\text{HO}_2)$ and may be associated with the lower polarity of these
326 molecules compared to HO_2 . It is likely that, as with uptake of HO_2 , both N_2O_5 and ClONO_2 react with TiO_2 via
327 complexing with bridging OH groups and adsorbed H_2O , therefore less polar molecules will be less bound to the
328 surface and more likely to desorb back into the gas phase, leading to a smaller γ . The dependence of $\gamma(\text{N}_2\text{O}_5)$ for
329 TiO_2 with RH is also different to that for HO_2 observed here, with a small decrease of $\gamma(\text{N}_2\text{O}_5)$ observed as the RH is
330 increased from $\sim 5 - 23\%$ where a minimum is reached, then beyond 23% $\gamma(\text{N}_2\text{O}_5)$ increases as RH is increased.
331 (Tang et al., 2014). Competition between water and N_2O_5 for surface active OH groups was suggested for the initial
332 observed decrease in $\gamma(\text{N}_2\text{O}_5)$ with RH, whereas for $\text{RH} > \sim 23\%$ heterogeneous hydrolysis of N_2O_5 to form HNO_3
333 starts to drive reactive uptake resulting in an increase of $\gamma(\text{N}_2\text{O}_5)$ (Tang et al., 2014). Measurements of $\gamma(\text{ClONO}_2)$
334 onto TiO_2 particles were only made at two values of RH, insufficient to determine any systematic dependence,
335 although Tang *et al.* (2016) expected $\gamma(\text{ClONO}_2)$ to increase as more water adsorbs onto the surface of TiO_2 particles.

336 George et al. (2013) previously measured $\gamma(\text{HO}_2)$ onto dry salt aerosols. Values of $\gamma(\text{HO}_2)$ for NaCl and $(\text{NH}_4)_2\text{SO}_4$
337 at RH values ($33 - 54\%$) below their deliquescence point were below the limit of detection ($\gamma(\text{HO}_2) < 0.004$). Values
338 of $\gamma(\text{HO}_2)$ for TiO_2 reported here (Figure 4 and Table 1) are more than an order of magnitude greater than that of
339 solid salts, even for $\text{RH} = 11\%$. A possible explanation for the difference in $\gamma(\text{HO}_2)$ values could be that even though
340 the sizes of the aerosols determined by the SMPS are similar, dry salt aerosols are more spherical in shape than TiO_2
341 particles which may be more fractal in nature. As the SMPS indirectly measures the surface area of aerosols by



342 measuring their mobility through an electric field, an assumption that the aerosol is spherical has to be made. If this
343 is not the case, this may lead to a significant under-prediction of the surface area of non-spherical aerosols and
344 therefore an over-prediction of $\gamma(\text{HO}_2)$. In order to measure the geometry of the TiO_2 particles, a scanning electron
345 microscope (SEM, FEI Nova NanoSEM 450) operating at 3 kV was used to image the TiO_2 nanoparticles used within
346 these experiments. Samples for the SEM were prepared by dispersing the nanoparticles in ethanol and allowing a
347 drop of this solution to dry on a silicon wafer. The wafer with nanoparticles was then mounted on SEM stubs using
348 conductive carbon tapes and coated with 2 nm of Ir, using a Cressington 208HR high resolution sputter coater. Figure
349 7 shows an example of an SEM image providing evidence that the TiO_2 particles are spherical and therefore any error
350 associated with SMPS measurements of surface area is minimal. A more likely explanation for the higher $\gamma(\text{HO}_2)$
351 for TiO_2 particles is that dry salt aerosols do not adsorb a significant amount of water onto their surface until the
352 deliquescence point reached, whereas at $\text{RH} = 11\%$ Figure 4 shows that the TiO_2 particles already have a monolayer
353 coverage which can form relatively strongly bound complexes with HO_2 . Measurements of $\gamma(\text{HO}_2)$ onto aqueous salt
354 aerosols show that $\gamma(\text{HO}_2)$ significantly increases above the deliquescence point (George et al., 2013) and is
355 comparable to $\gamma(\text{HO}_2)$ measured for TiO_2 ($\gamma(\text{HO}_2) \sim 0.01$).



356

357 **Figure 7.** SEM image of a single TiO_2 particle magnified 80,000 \times used within this study.

358 **3.3 Implications of HO_2 uptake by TiO_2 for stratospheric chemistry**

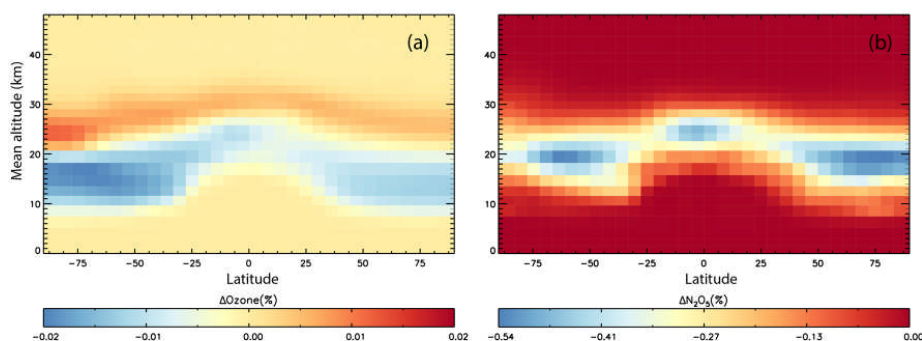
359 The effect of HO_2 uptake onto TiO_2 particles upon the stratospheric concentrations of HO_2 and O_3 was assessed using
360 the TOMCAT model (Chipperfield, 1999, 2006). At RH relevant to the lower stratosphere ($< 40\%$) the measurements
361 showed that $\gamma(\text{HO}_2)$ is in the range 0.020 - 0.028 at 295 K. An inverse temperature dependence of $\gamma(\text{HO}_2)$ onto dry
362 sea-salt aerosols has previously been observed (Remorov et al., 2002), and although there have been no systematic
363 experimental studies of the temperature dependence of $\gamma(\text{HO}_2)$, parameterisations have developed (Thornton et al.,
364 2008; Macintyre and Evans, 2011). At stratospherically relevant temperatures ($T = 200 - 220$ K), $\gamma(\text{HO}_2)$ is likely to
365 be considerably larger than observed at 295 K, however it is not possible to cool the aerosol flow tube/SMPS system
366 to verify this experimentally. Therefore $\gamma(\text{HO}_2) = 1$ was used in the model simulations representing an upper limit,



367 with three TOMCAT simulations performed as follows. A control simulation, similar to that presented in
368 Chipperfield et al. (2015) did not include TiO₂ particles. A specified latitude-height distribution of TiO₂ particles was
369 then included in two simulations with an effective aerosol surface area density equal to that of sulphate aerosols in
370 1992 the year after the eruption of Mt. Pinatubo. This is an assumption which allows for the fact that less TiO₂ mass
371 is needed in order to produce the same radiative impact as sulphate aerosol from Mt. Pinatubo, but the TiO₂ particle
372 size is smaller. Hence these effects largely cancel (Tang et al., 2014). Stratospheric injection via a geo-engineering
373 solution will result initially in a different distribution of TiO₂ particles compared with after the Mt. Pinatubo eruption,
374 but it is assumed that following mixing and transport the distributions would resemble one another and not lead to
375 any significant difference in model behaviour and the conclusions drawn. Support from this assumption comes from
376 a model run in which a globally uniform distribution of TiO₂ was assumed initially and which yielded very similar
377 results.

378 The first of these simulations included only the loss of N₂O₅ on TiO₂ particles with $\gamma(\text{N}_2\text{O}_5) = 0.005$, the upper limit
379 used in the modelling of Tang et al. (2014), which allows us to compare our results with their study. The second TiO₂
380 simulation also included the loss of HO₂ on TiO₂ particles with a $\gamma(\text{HO}_2) = 1$, as discussed above. Figure 8 shows
381 the impact of including heterogeneous loss of N₂O₅ on TiO₂ particles in the model.

382



383

384 **Figure 8.** Annual mean change (%) in atmospheric O₃ (a) and N₂O₅ (b) calculated using the TOMCAT 3-D model
385 from inclusion of heterogeneous loss of N₂O₅ on TiO₂ particles for 2008 and using $\gamma(\text{N}_2\text{O}_5) = 0.005$.

386

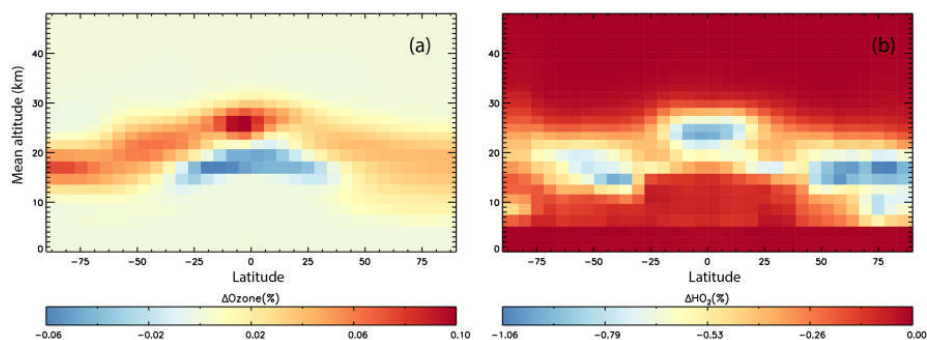
387 N₂O₅ is decreased by up to 0.5% in the region of TiO₂ particles, which is assumed to follow the distribution of
388 sulphate particles after the Mt. Pinatubo eruption, in order follow the approach of previous modelling studies.
389 Assuming a globally uniform distribution initially yielded results that were very similar. Inclusion of uptake is only
390 a minor effect and considerably smaller than the impact of around -20% modelled by Tang et al. (2004) for the same
391 assumed $\gamma(\text{N}_2\text{O}_5) = 0.005$. The reasons for this are not clear, although it is noted that the effect modelled in our off-
392 line chemical transport model, with specified meteorology, is clearly confined to regions of high aerosol loading.



393 The impacts modelled in the nudged chemistry-climate model study of Tang et al. (2004) are not confined to the
394 region of high aerosol and even extend to the upper stratosphere. It is possible that their simulations, although nudged,
395 also include some dynamical feedback which enhances an otherwise small signal. Figure 8 also shows that the
396 resulting impact on O₃ is small with changes less than 0.02%. The model produces a region of slight decrease in the
397 very low stratosphere, with a region of slight increase above.

398 Figure 9 shows results from the simulation which also included the loss of HO₂ on stratospheric TiO₂ particles, and
399 using $\gamma(\text{HO}_2) = 1$ (a simulation using the measured value of $\gamma(\text{HO}_2) = 0.021$ at 295 K led to no impact on O₃ or HO₂).

400



401

402 **Figure 9.** Annual mean change (%) in atmospheric O₃ (a) and HO₂ (b) calculated using the TOMCAT 3-D model
403 from inclusion of heterogeneous loss of HO₂ on TiO₂ particles for 2008, and using $\gamma(\text{HO}_2) = 1$.

404

405 It is evident that HO₂ loss due to heterogeneous reaction between HO₂ and TiO₂ particles in 2008 is < 1% and is
406 confined to the lower stratosphere where it is assumed TiO₂ particles are located. Figure 9 also shows that the
407 subsequent effect of the TiO₂ particles on the O₃ concentrations through the effects of this reaction is also small
408 (< 0.1%), with a small decrease in the tropical upper troposphere/lower stratosphere and a small increase at all
409 latitudes in the lower stratosphere. This small effect of TiO₂ particles on stratospheric HO₂ and O₃ concentrations is
410 due to the reactive nature and short lifetime of HO₂. The species readily reacts with other gas phase species (e.g. O₃)
411 and so loss on TiO₂ surfaces does not compete significantly.

412

413 4. Conclusions and further work

414 The reactive uptake coefficients for the heterogeneous reaction of HO₂ onto TiO₂ particles were measured at different
415 RH and at room temperature for the first time using an aerosol flow tube reactor coupled with a sensitive FAGE HO₂
416 detection system. A range of HO₂ uptake coefficients on TiO₂ particles were measured varying from $\gamma(\text{HO}_2) = 0.021$
417 ± 0.001 to 0.036 ± 0.007 for RH over the range 11% to 66%, respectively. The HO₂ uptake coefficient showed a



418 positive dependence on RH which correlated well with the number of monolayers of water adsorbed onto the TiO₂
419 particle. These results suggest a mechanism by which HO₂ adsorbs to the surface of the TiO₂ particle by forming
420 complexes with water molecules bound to bridging OH groups. As the number of water layers increases so does the
421 network of hydrogen bonds that stabilises HO₂ leading to a longer adsorption lifetime and increased $\gamma(\text{HO}_2)$. The
422 TOMCAT chemical transport model was used to evaluate the possible effects of HO₂ uptake (using an upper limit of
423 $\gamma(\text{HO}_2) = 1$) onto the surface of TiO₂ particles on the stratospheric concentrations of HO₂ and O₃. The amount of
424 TiO₂ used was chosen to achieve a similar cooling to that following the Mt. Pinatubo eruption, but the model predicted
425 a very small loss of both stratospheric HO₂ and O₃. TiO₂ possesses photocatalytic properties and water adsorbed
426 onto its surface may dissociate under stratospheric illumination providing a source of radicals (Chen et al.,
427 2012; Romanias et al., 2012). Production of OH and HO₂ from irradiated TiO₂ surfaces should be evaluated in future
428 studies to fully understand the consequences of injection of TiO₂ particles into the stratosphere.

429

430 **Acknowledgements**

431 We are grateful to the Natural Environment Research Council for funding a studentship (DRM) and for funding the
432 aerosol flow tube apparatus (grant number NE/F020651/1)). LKW, TI, PWS and DEH are also grateful to the
433 NERC funded National Centre for Atmospheric Science for ongoing support. The TOMCAT modelling work was
434 supported by the EU StratoClim project (FP7 grant 603557). We thank Wuhu Feng (NCAS Leeds) for help with the
435 model. The model simulations were performed on the University of Leeds and N8 HPC system.

436

437 **References**

- 438 Aloisio, S., and Francisco, J. S.: Existence of a hydroperoxy and water (HO₂.H₂O) radical complex, *Journal of*
439 *Physical Chemistry A*, 102, 1899-1902, 10.1021/jp972173p, 1998.
- 440 Ammann, M., Cox, R. A., Crowley, J. N., Jenkin, M. E., Mellouki, A., Rossi, M. J., Troe, J., and Wallington, T. J.:
441 Evaluated kinetic and photochemical data for atmospheric chemistry: Volume VI - heterogeneous reactions with
442 liquid substrates, *Atmos Chem Phys*, 13, 8045-8228, 10.5194/acp-13-8045-2013, 2013.
- 443 Anpo, M., Che, M., Fubini, B., Garrone, E., Giamello, E., and Paganini, M. C.: Generation of superoxide ions at
444 oxide surfaces, *Topics in Catalysis*, 8, 189, 10.1023/a:1019117328935, 1999.
- 445 Bahrini, C., Parker, A., Schoemaeker, C., and Fittschen, C.: Direct detection of HO₂ radicals in the vicinity of
446 TiO₂ photocatalytic surfaces using cw-CRDS, *Appl. Catal. B-Environ.*, 99, 413-419,
447 10.1016/j.apcatb.2010.06.040, 2010.
- 448 Bedjanian, Y., Romanias, M. N., and El Zein, A.: Uptake of HO₂ radicals on Arizona Test Dust, *Atmos Chem*
449 *Phys*, 13, 6461-6471, 10.5194/acp-13-6461-2013, 2013.
- 450 Brown, R. L.: Tubular flow reactors with 1st-order kinetics, *Journal of Research of the National Bureau of*
451 *Standards*, 83, 1-8, 1978.
- 452 Chen, H., Nanayakkara, C. E., and Grassian, V. H.: Titanium Dioxide Photocatalysis in Atmospheric Chemistry,
453 *Chem. Rev.*, 112, 5919-5948, 10.1021/cr3002092, 2012.
- 454 Chipperfield, M. P.: Multiannual simulations with a three-dimensional chemical transport model, *J. Geophys. Res.-*
455 *Atmos.*, 104, 1781-1805, 10.1029/98jd02597, 1999.
- 456 Chipperfield, M. P.: New version of the TOMCAT/SLIMCAT off-line chemical transport model: Intercomparison
457 of stratospheric tracer experiments, *Q. J. R. Meteorol. Soc.*, 132, 1179-1203, 10.1256/qj.05.51, 2006.
- 458 Chipperfield, M. P., Dhomse, S. S., Feng, W., McKenzie, R. L., Velders, G. J. M., and Pyle, J. A.: Quantifying the
459 ozone and ultraviolet benefits already achieved by the Montreal Protocol, *Nat. Commun.*, 6, 8,
460 10.1038/ncomms8233, 2015.
- 461 Dutton, E. G., and Christy, J. R.: Solar radiative forcing at selected locations and evidence for global lower
462 tropospheric cooling following the eruptions of El-Chichon and Pinatubo, *Geophysical Research Letters*, 19,
463 2313-2316, 10.1029/92gl02495, 1992.
- 464 Fuchs, N. A., and Sutugin, A. G.: Highly dispersed aerosols, *Ann Arbor Science*, London, 1970.
- 465 George, I. J., Matthews, P. S., Whalley, L. K., Brooks, B., Goddard, A., Baeza-Romero, M. T., and Heard, D. E.:
466 Measurements of uptake coefficients for heterogeneous loss of HO₂ onto submicron inorganic salt aerosols,
467 *Phys Chem Chem Phys*, 15, 12829-12845, 10.1039/c3cp51831k, 2013.
- 468 Goodman, A. L., Bernard, E. T., and Grassian, V. H.: Spectroscopic study of nitric acid and water adsorption on
469 oxide particles: Enhanced nitric acid uptake kinetics in the presence of adsorbed water, *Journal of Physical*
470 *Chemistry A*, 105, 6443-6457, 10.1021/jp0037221, 2001.
- 471 Gustafsson, R. J., Orlov, A., Badger, C. L., Griffiths, P. T., Cox, R. A., and Lambert, R. M.: A comprehensive
472 evaluation of water uptake on atmospherically relevant mineral surfaces: DRIFT spectroscopy,
473 thermogravimetric analysis and aerosol growth measurements, *Atmos Chem Phys*, 5, 3415-3421, 2005.
- 474 Heard, D. E., and Pilling, M. J.: Measurement of OH and HO₂ in the troposphere, *Chem. Rev.*, 103, 5163-5198,
475 2003.
- 476 Holloway, A. M., and Wayne, R. P.: *Atmospheric Chemistry*, Royal Society of Chemistry, 2010.
- 477 Huneus, N., Schulz, M., Balkanski, Y., Griesfeller, J., Prospero, J., Kinne, S., Bauer, S., Boucher, O., Chin, M.,
478 Dentener, F., Diehl, T., Easter, R., Fillmore, D., Ghan, S., Ginoux, P., Grini, A., Horowitz, L., Koch, D., Krol,
479 M. C., Landing, W., Liu, X., Mahowald, N., Miller, R., Morcrette, J. J., Myhre, G., Penner, J., Perlwitz, J., Stier,
480 P., Takemura, T., and Zender, C. S.: Global dust model intercomparison in AeroCom phase I, *Atmos Chem*
481 *Phys*, 11, 7781-7816, 10.5194/acp-11-7781-2011, 2011.
- 482 Joshi, R., and Ghanty, T. K.: Hydrogen bonding interaction between HO₂ radical and selected organic acids,
483 RCOOH (R = CH₃, H, Cl and F), *Chem. Phys. Lett.*, 584, 43-48, 10.1016/j.cplett.2013.08.025, 2013.
- 484 Karagulian, F., Santschi, C., and Rossi, M. J.: The heterogeneous chemical kinetics of N₂O₅ on CaCO₃ and other
485 atmospheric mineral dust surrogates, *Atmos Chem Phys*, 6, 1373-1388, 2006.
- 486 Ketteler, G., Yamamoto, S., Bluhm, H., Andersson, K., Starr, D. E., Ogletree, D. F., Ogasawara, H., Nilsson, A.,
487 and Salmeron, M.: The nature of water nucleation sites on TiO₂(110) surfaces revealed by ambient pressure X-
488 ray photoelectron spectroscopy, *J. Phys. Chem. C*, 111, 8278-8282, 10.1021/jp068606i, 2007.
- 489 Lakey, P. S. J., George, I. J., Baeza-Romero, M. T., Whalley, L. K., and Heard, D. E.: Organics Substantially
490 Reduce HO₂ Uptake onto Aerosols Containing Transition Metal ions, *Journal of Physical Chemistry A*, 120,
491 1421-1430, 10.1021/acs.jpca.5b06316, 2016.



- 492 Macintyre, H. L., and Evans, M. J.: Parameterisation and impact of aerosol uptake of HO₂ on a global tropospheric
 493 model, *Atmos Chem Phys*, 11, 10965-10974, 10.5194/acp-11-10965-2011, 2011.
- 494 Matthews, P. S. J., Baeza-Romero, M. T., Whalley, L. K., and Heard, D. E.: Uptake of HO₂ radicals onto Arizona
 495 test dust particles using an aerosol flow tube, *Atmos Chem Phys*, 14, 7397-7408, 10.5194/acp-14-7397-2014,
 496 2014.
- 497 McCormick, M. P., Thomason, L. W., and Trepte, C. R.: Atmospheric effects of the Mt. Pinatubo eruption, *Nature*,
 498 373, 399-404, 10.1038/373399a0, 1995.
- 499 Pope, F. D., Braesicke, P., Grainger, R. G., Kalberer, M., Watson, I. M., Davidson, P. J., and Cox, R. A.:
 500 Stratospheric aerosol particles and solar-radiation management, *Nat. Clim. Chang.*, 2, 713-719,
 501 10.1038/nclimate1528, 2012.
- 502 Remorov, R. G., Gershenson, Y. M., Molina, L. T., and Molina, M. J.: Kinetics and mechanism of HO₂ uptake on
 503 solid NaCl, *Journal of Physical Chemistry A*, 106, 4558-4565, 10.1021/jp013179o, 2002.
- 504 Romanias, M. N., El Zein, A., and Bedjanian, Y.: Heterogeneous Interaction of H₂O₂ with TiO₂ Surface under Dark
 505 and UV Light Irradiation Conditions, *Journal of Physical Chemistry A*, 116, 8191-8200, 10.1021/jp305366v,
 506 2012.
- 507 Shepherd, J. G., and Working Group on Geoengineering the Climate: Geoengineering the climate: science,
 508 governance and uncertainty, Project Report, 2009.
- 509 Tang, M., Keeble, J., Telford, P. J., Pope, F. D., Braesicke, P., Griffiths, P. T., Abraham, N. L., McGregor, J.,
 510 Watson, I. M., Cox, R. A., Pyle, J. A., and Kalberer, M.: Heterogeneous reaction of ClONO₂ with TiO₂ and SiO₂
 511 aerosol particles: implications for stratospheric particle injection for climate engineering, *Atmos. Chem. Phys.*,
 512 16, 15397-15412, 10.5194/acp-16-15397-2016, 2016.
- 513 Tang, M. J., Telford, P. J., Pope, F. D., Rkiouak, L., Abraham, N. L., Archibald, A. T., Braesicke, P., Pyle, J. A.,
 514 McGregor, J., Watson, I. M., Cox, R. A., and Kalberer, M.: Heterogeneous reaction of N₂O₅ with airborne TiO₂
 515 particles and its implication for stratospheric particle injection, *Atmos Chem Phys*, 14, 6035-6048, 10.5194/acp-
 516 14-6035-2014, 2014a.
- 517 Tang, M. J., Telford, P. J., Pope, F. D., Rkiouak, L., Abraham, N. L., Archibald, A. T., Braesicke, P., Pyle, J. A.,
 518 McGregor, J., Watson, I. M., Cox, R. A., and Kalberer, M.: *Corrigendum to* Heterogeneous reaction of N₂O₅
 519 with airborne TiO₂ particles and its implication for stratospheric particle injection, *Atmos Chem Phys*, 14, 8233-
 520 8234, 10.5194/acp-14-8233-2014, 2014b.
- 521 Textor, C., Schulz, M., Guibert, S., Kinne, S., Balkanski, Y., Bauer, S., Bernsten, T., Berglen, T., Boucher, O.,
 522 Chin, M., Dentener, F., Diehl, T., Easter, R., Feichter, H., Fillmore, D., Ghan, S., Ginoux, P., Gong, S.,
 523 Kristjansson, J. E., Krol, M., Lauer, A., Lamarque, J. F., Liu, X., Montanaro, V., Myhre, G., Penner, J., Pitari,
 524 G., Reddy, S., Seland, O., Stier, P., Takemura, T., and Tie, X.: Analysis and quantification of the diversities of
 525 aerosol life cycles within AeroCom, *Atmos Chem Phys*, 6, 1777-1813, 2006.
- 526 Thornton, J., and Abbatt, J. P. D.: Measurements of HO₂ uptake to aqueous aerosol: Mass accommodation
 527 coefficients and net reactive loss, *J. Geophys. Res.-Atmos.*, 110, 10.1029/2004jd005402, 2005.
- 528 Thornton, J. A., Jaegle, L., and McNeill, V. F.: Assessing known pathways for HO₂ loss in aqueous atmospheric
 529 aerosols: Regional and global impacts on tropospheric oxidants, *J. Geophys. Res.-Atmos.*, 113,
 530 10.1029/2007jd009236, 2008.
- 531 Usher, C. R., Michel, A. E., Stec, D., and Grassian, V. H.: Laboratory studies of ozone uptake on processed mineral
 532 dust, *Atmos. Environ.*, 37, 5337-5347, 10.1016/j.atmosenv.2003.09.014, 2003.
- 533 Versick, S., Stiller, G. P., von Clarmann, T., Reddmann, T., Glatthor, N., Grabowski, U., Hoepfner, M., Kellmann,
 534 S., Kiefer, M., Linden, A., Ruhnke, R., and Fischer, H.: Global stratospheric hydrogen peroxide distribution
 535 from MIPAS-Envisat full resolution spectra compared to KASIMA model results, *Atmos Chem Phys*, 12, 4923-
 536 4933, 10.5194/acp-12-4923-2012, 2012.
- 537 Wennberg, P. O., Cohen, R. C., Stimpfle, R. M., Koplow, J. P., Anderson, J. G., Salawitch, R. J., Fahey, D. W.,
 538 Woodbridge, E. L., Keim, E. R., Gao, R. S., Webster, C. R., May, R. D., Toohey, D. W., Avallone, L. M.,
 539 Proffitt, J. A., Loewenstein, M., Podolske, J. R., Chan, K. R., Wofsy, S. C.: Removal of stratospheric O₃ by
 540 radicals - in situ measurements of OH, HO₂, NO, NO₂, ClO, and BrO, *Science*, 266, 398-404,
 541 10.1126/science.266.5184.398, 1994.
- 542 Winiberg, F. A. F., Smith, S. C., Bejan, I., Brumby, C. A., Ingham, T., Malkin, T. L., Orr, S. C., Heard, D. E., and
 543 Seakins, P. W.: Pressure-dependent calibration of the OH and HO₂ channels of a FAGE HO_x instrument using
 544 the Highly Instrumented Reactor for Atmospheric Chemistry (HIRAC), *Atmos. Meas. Tech.*, 8, 523-540,
 545 10.5194/amt-8-523-2015, 2015.



546 Yamamoto, S., Bluhm, H., Andersson, K., Ketteler, G., Ogasawara, H., Salmeron, M., and Nilsson, A.: In situ x-
547 ray photoelectron spectroscopy studies of water on metals and oxides at ambient conditions, *J. Phys.-Condes.*
548 *Matter*, 20, 14, 10.1088/0953-8984/20/18/184025, 2008.

549